ISSI Visiting Scientists Programme

THE RHESSI MISSION: X-RAY SPECTRA AND IMAGE ANALYSIS BY MEANS OF INVERSION METHODS.

Team Leader: Anna Maria Massone
(CNR-INFM LAMIA, Genova, Italy)

Report of the Second Group Meeting:
January 12-18, 2005

SPECTROSCOPY

Isotropic albedo contribution in RHESSI spectra

During this meeting J. Kašparová and E. Kontar continued in the analysis of isotropic albedo contribution in RHESSI spatially integrated spectra. Albedo is formed by the primary flare photons scattered in the photosphere and modifies the mean electron flux distribution $\bar{F}(E)$ determined from the observed total photon spectra, i.e. from the primary plus scattered component.

They focused mainly on the distribution of spectral indices of total photon spectra with respect to the flare position on the solar disc. Using all suitable RHESSI flares detected above 50 keV, they found that only spectral index at $\sim$ 20 keV shows tendency of being spatially dependent, see Figure 1.

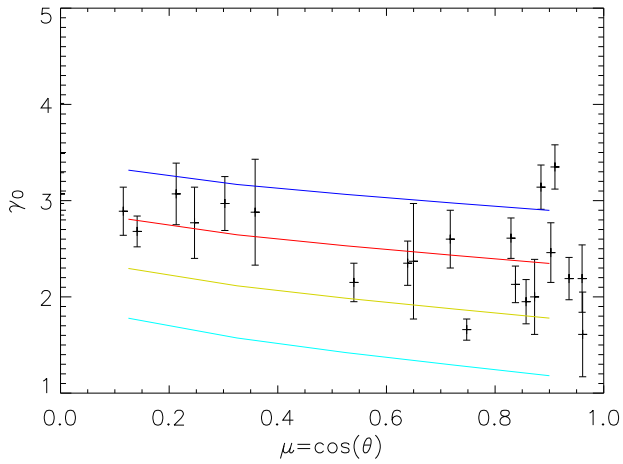

Fig. 1.— Spectral index γ_0 at the 15 - 20 keV range as a function of heliocentric angle ($\mu = \cos\theta$). Colour lines (cyan, yellow, red, and blue) indicate models with primary single power-law spectrum: $\gamma_p = 2.0$, 2.5, 3.0, and 3.5, respectively.

This is consistent with modelled influence of albedo which predicts the largest deviation between the primary γ_p and total γ photon spectral indices at energies below 20 keV, where $\gamma < \gamma_p$. However, γ_p strongly depends on γ which can vary with energy and from flare to flare. The effect of albedo is more pronounced for flatter primary spectra, therefore the analysis was limited to flares with $\gamma < 3.5$. Other difficulty is connected with the thermal component which can contribute to the photon spectrum at these energies and "mask" the albedo component. Thus, the flares with substational thermal component were excluded from

the analysis. The resulting sample of flares is not large ($\sim$ 25 flares), data show scatter, and subsequently the spatial dependecy of γ cannot be regarded as confirmed yet. Therefore, it was decided to extend the analysis also to the RHESSI flares detected only up to 50 keV in order to increase the number events.

On the other hand, the flattest total photon spectra or those with the largest change in spectral indices at different energy ranges are consistent with a dip in $\bar{F}(E)$ below $\sim$ 20 keV. All such dips are found only for flares on the solar disc and all of the dips can be removed by taking into account the isotropic albedo contribution relevant to the flare position on the disc, see Figure 2.

To determine $\bar{F}(E)$, a new version of regularisation software developed by E. Kontar was used. The software is designed to find $\bar{F}(E)$ directly from the detected RHESSI count flux, i.e. it does not require a conversion of the data into photon flux prior to the regularisation. The resulting $\bar{F}(E)$ are consistent with those obtained by the regularisation software of A. M. Massone (regularised $\bar{F}(E)$ from photon flux).

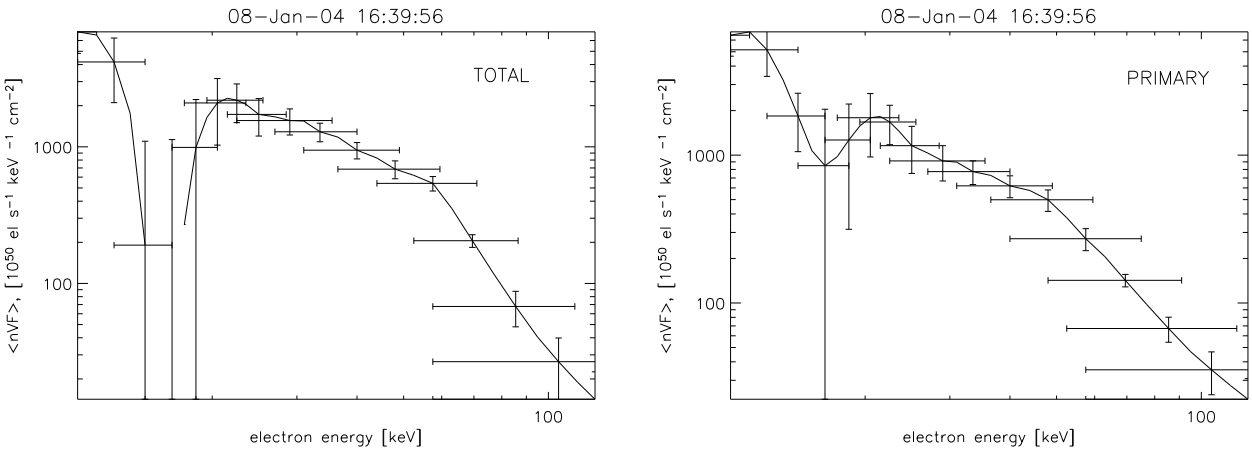

Fig. 2.— Regularised $\bar{F}(E)$ of the flare on Jan 8, 2004 determined using total (left) and primary (right) count spectra. Notice the dip below $\sim$ 20 keV for the case of total spectra.

Influence of systematic errors in the photon spectrum on the inversion

Monte Carlo techniques were used to calculate plausible systematic errors in the photon spectrum. These errors had an rms deviation of 5% and were correlated over energy ranges so that they would represent credible calibration-based errors in the photon spectrum (Figure 3 shows plots of the error factors as a function of energy). These factors were used to multiply

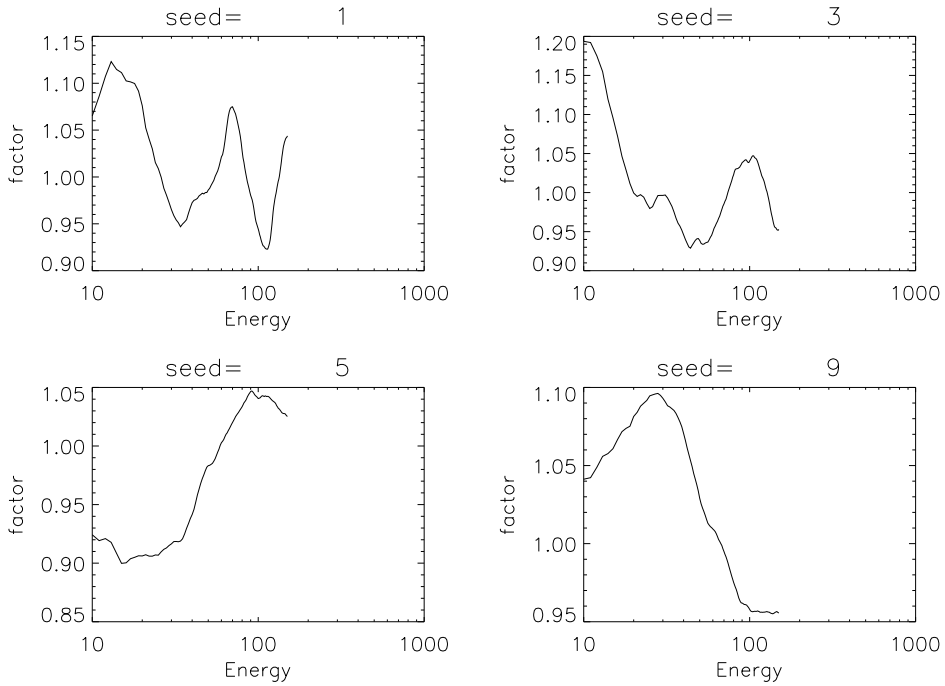

Fig. 3.— Simulated error factors as a function of energy. Top left panel: factor 1. Top right panel: factor 2. Bottom left panel: factor 3. Bottom right panel: factor 4.

a real photon spectrum. The original and four distorted photon spectra were each inverted to corresponding electron spectra using the inversion software. Comparison of the four *distorted* electron spectra (hereafter referred to as F_1, F_2, F_3, F_4) with the *original* (F_0), showed rms differences of between 6% and 10%, as shown in Table 1. The conclusion was that unknown calibration errors would not be unduly magnified by spectral inversion.

	Mean Value	Standard Deviation
F_1/F_0	1.003	0.091
F_2/F_0	0.987	0.080
F_3/F_0	1.001	0.067
F_4/F_0	0.993	0.069

Table 1: Comparison of the four distorted electron spectra with the original.

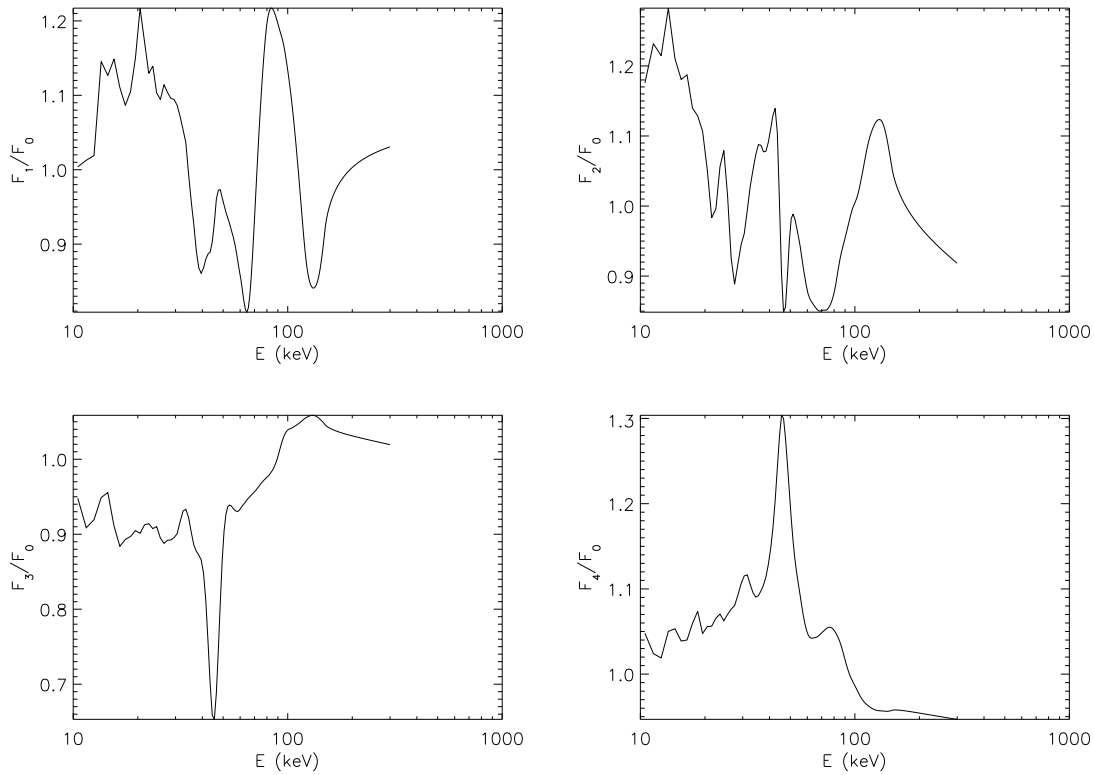

Fig. 4.— Reconstructed error factors as a function of energy.

Reconstruction of the differential emission measure

Under a purely thermal interpretation of an observed solar hard X-ray bremsstrahlung spectrum, it can be shown [1] that the differential emission measure $\xi(T)$ is related to the mean electron spectrum $\bar{F}(E)$ by the equation

$$\bar{F}(E) = \frac{2^{3/2}E}{(\pi m_e)^{1/2}} \int_0^\infty \frac{\xi(T)}{(kT)^{3/2}} e^{-E/kT} dT \tag{1}$$

where T is the temperature and k is the Boltzmann constant.

A completely rigorous description of the thermal model then requires the introduction of two integral equations. First, the (isotropic) source-averaged effective electron flux spectrum $\overline{F}(E)$, is related to the photon spectrum by means of the Volterra integral equation

$$I(\epsilon) = \frac{\overline{n}V}{4\pi R^2} \int_\epsilon^\infty \overline{F}(E) Q(\epsilon, E) dE \quad , \tag{2}$$

with a fully correct form of $Q(\epsilon, E)$. Second, the inversion of Eq. 1 allows to recover $\xi(T)$ from $\overline{F}(E)$.

However a basic technical difficulty is due to the fact that solving the second inverse problem is extremely problematic. Simple changes of variables reduce this problem to a Laplace transform inversion problem with noisy data. Most inversion methods for the real Laplace transform have been formulated within the framework of regularization theory for ill-posed inverse problems. At the core of these approaches there is the search for an optimal trade-off between stability against unphysical oscillations and accurate reproducibility of the data. Such an optimization result is obtained either by fixing a real positive regularization parameter in Tikhonov-like methods [4] or by applying some stopping rule to iterative procedures. However, the present application is particularly challenging owing to the particular nature of the solar spectral data involved here. Typical solar $\overline{F}(E)$ are characterized by a large dynamic range (at least three orders of magnitude for around one order of magnitude in the E range) and, more significantly, the corresponding $\xi(T)$ have completely different forms at low and high T: at small T, a near thermal (δ function) component which differs from zero only in a small T range (narrow support); at high T, a monotonic component spread over a large interval. A consequence of this complexity in the source function is that regularization approaches may lose some (or most) of their effectiveness. For example, the reconstruction of $\xi(T)$ at low T with classical Tikhonov regularization may correctly reproduce the location of the temperature peak but typically presents ringing effects whose negative components, which are numerical artefacts, may induce to conclude that the spectrum is not thermally interpretable. Negative ringing can be eliminated by applying a reconstruction method with positivity constraint. However such an approach is not effective while recovering the high temperature part of $\xi(T)$ which has a power-law-like behavior and requires regularization methods with more smoothing power. To deal with these kinds of difficulty, we have utilized the following approach: an iterative scheme with positivity constraint (projected Landweber method [3]) is applied for the inversion of the low energy part of $\overline{F}(E)$, in order to eliminate unphysical ringing effects with negative oscillations in the reconstruction of the part of $\xi(T)$ characterized by a narrow support; then, a first order Tikhonov regularization method is applied for the inversion of the high-energy part of $\overline{F}(E)$, where an appropriate boundary condition constrains the reconstructed $\xi(T)$ to behave well (i.e., with a slope compatible with the spectral index of the photon data) at high T. The two reconstructed $\xi(T)$ are then connected together noting that each inverted part of $\overline{F}(E)$, if known with sufficient precision, could in principle provide information on $\xi(T)$ in the whole T range.

In Fig. 5 a simple example is considered in which the simulated differential emission measure (solid line) comprises an isothermal component (at $T_0 = 4$keV) at low electron energies plus a power law behavior at high energies.

In real $\overline{F}(E)$, energies up to typically 10 keV must be avoided owing to the presence of (or problematical correction for) lines of non-bremsstrahlung origin or to systematic errors

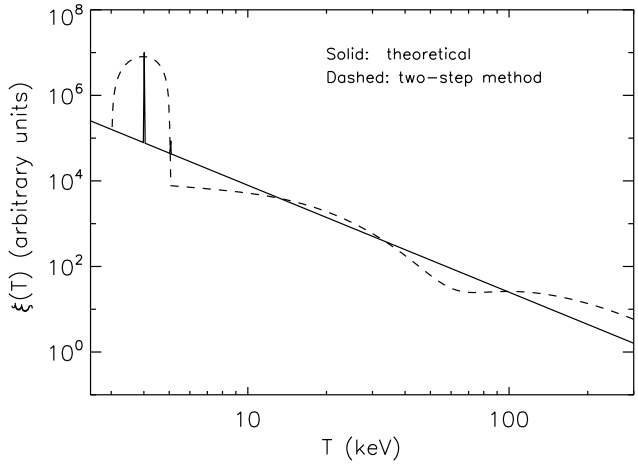

Fig. 5.— Inversion of $\overline{F}(E)$ corresponding to the theoretical $\xi(T)$ plotted in solid line. Reconstruction (dashed) obtained by inverting the low-energy part of the electron spectrum with the projected Landweber method and the high-energy part with first order Tikhonov regularization and by connecting the two restorations.

introduced by the hardware. In other words, a typical experimental situation is that $\overline{F}(E)$ is inverted from electron energies bigger than the temperatures involved in the thermal process. In order to study the effect of this on the inversion method, we considered the test shown in Fig. 6. The electron spectrum corresponding to an isothermal $\xi(T)$ with $T_0 = 7$ keV is inverted for different electron energy sampling ranges: $2-20$ keV (solid), $2-7$ keV (dashed), $7-20$ keV (dotted) and $20-70$ keV (dot-dashed). Defining the "centroid" temperature of the reconstructed distributions by $< T >= \int T\xi(T)dT / \int \xi(T)dT$ and T_{max} as the temperature at which the recovered $\xi(T)$ peaks, we found that if T_0 is higher than the energy range considered, the reconstruction preserves the symmetry of the δ-function (so that T_{max} and $< T >$ more or less coincide) but the peak temperature is notably overestimated (almost 20%). If T_0 is smaller than the sampled energies (which is the realistic situation), the reconstruction is rather skewed (in such a way that T_{max} is bigger than $< T >$, as opposed to the case of Tikhonov regularization), presents a widened Full Width at Half Maximum (FWHM) and the peak temperature is slightly underestimated: for example, if the selected range is $20 - 70$ keV, the reconstructed T_{max} is $\sim 5\%$ smaller than the true one.

After the meeting a fully revised version of the paper *Regularized reconstruction of the differential emission measure from solar flare hard X-ray spectra*, has been submitted to *Solar Physics*.

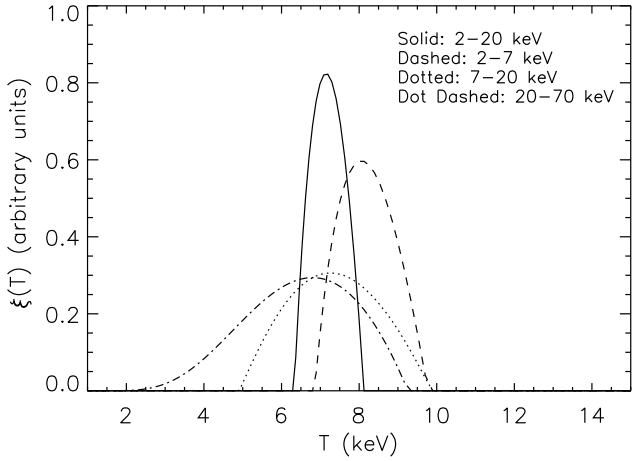

Fig. 6.— Reconstruction of a δ-function peaked at $T_0 = 7$ keV when the corresponding $\overline{F}(E)$ is sampled over different electron energy ranges: $2 - 20$ keV (solid); $2 - 7$ keV (dashed); $7 - 20$ keV (dotted); $20 - 70$ keV (dot-dashed). The reconstruction method is the projected Landweber method with positivity.

IMAGING

For this meeting Dr. Gordon J. Hurford (Space Sciences Laboratory - University of California at Berkeley), RHESSI leading scientist for the imaging problem [2], joined the team. As far as the problem of image construction from raw RHESSI data using regularization techniques, our results have been so far exploratory.

REFERENCES

[1] Brown J.C., 1974, in G.A. Newkirk (ed.) Coronal Disturbances. *IAU Symp.* **57**, 395.

[2] Hurford, G. J. et al., 2002, Solar Phys., **210**, 61.

[3] Lagendijk, R., Biemond, J. and Boeckee, D. 1988, IEEE Trans. Acoust. Speech Signal Proc., **36**, 1874.

[4] Tikhonov A.N., 1963, Dokl. Akad. Nauk., USSR, **153**, 501-504.